Department of Biopharmaceutics[1], School of Pharmacy, Hyogo University of Health Sciences Hyogo; Department of Oral and Maxillofacial Anatomy[2], The Institute of Health Bioscience, The University of Tokushima Graduate School, Tokushima; Department of Hygiene Chemistry[3], School of Pharmacy, Ohu University, Fukushima Japan

Novel morphological features in the death of MCF-7 human breast cancer cells after exposure to anticancer drugs

F. KUGAWA[1], S.-O. DALKHUREN[2], A. UENO[3], K. YAMASHITA[2]

Received December 21, 2011, accepted February 2, 2012

Prof. Dr. Fumihiko Kugawa, Department of Biopharmaceutics[1], School of Pharmacy, Hyogo University of Health Sciences, 1-3-6 Minatojima, Chuo-Ku, Kobe, Hyogo 650-8530, Japan
jfkugawa@huhs.ac.jp

Pharmazie 67: 862–869 (2012) *doi: 10.1691/ph.2012.1165*

Cell death of human breast cancer cell line MCF-7/pDsRed2-Mito, caused by independent- or multi-administration of three anticancer drugs, cyclophosphamide [CPA], doxorubicin [DXR], and 5-fluorouracil [5-FU], was studied using fluorescence and electron microscopy. In our previous study using cell viability assays, microscopic inspection of heterochromatin condensation, a DNA fragmentation assay, and flow cytometric analyses, the death of MCF-7 cells was classified into two groups. The cell death induced by CPA or 5-FU was classified as apoptotic, while the cell death induced by DXR treatment or a mixture of all three anticancer drugs was classified as non-apoptotic. Here, we examined the morphology of the whole cell and its organelles, including the mitochondria, using electron microscopy. Mitochondria are of particular interest because they are the key organelle for the molecular apoptotic-death cascade. To monitor mitochondrial morphology, we used our previously constructed MCF-7/pDsRed2-Mito line, generated by introducing the pDsRed2-Mito® vector into MCF-7 cells. The mitochondria in these cells emit red fluorescence. We found that the administration of DXR alone or of all three anticancer drugs together resulted in the clumping of the red-fluorescent materials on both sides of the round dying cells, interrupted by the nucleus. Detailed electron microscopic observation revealed that the novel morphology of the dying MCF-7 cells might be owing, not to destruction of the mitochondrial membrane, but to the tight structure of the nuclear membrane. Other anticancer drugs showed different, characteristic features in electron microscopic images, which suggested that death induced by anti-cancer drugs in the human breast cancer cell line, MCF-7, may result from any of a number of diverse processes.

1. Introduction

Cyclophosphamide [CPA], doxorubicin [DXR], and 5-fluorouracil [5-FU] are among the most commonly used anti-breast cancer drugs, and they are usually administered together (Nagar 2010; Pal and Mortimer 2009; Perez and Muss 2005; Tokudome and Ito 2006). We previously studied the molecular mechanism for the cell death induced in human breast cancer by anticancer drugs. All three anti-cancer drugs mentioned above have long been recognized as "apoptosis-inducing" drugs (Derenzini et al. 2009; Zhang and Aft, 2009; Perik et al. 2006; Végran et al. 2006). However, three assays that are typically used to generate evidence for apoptotic events (condensed heterochromatin structure, DNA-ladder formation, and flow cytometric analysis) showed that the actions of these drugs were more complicated than expected (Kugawa et al. 2004b). Namely, treatment with either CPA or 5-FU caused apoptotic cell death in the human breast cancer cell line MCF-7. On the other hand, treatment with the individual drugs CPA, DXR, and 5-FU or their mixture (C + D + F) caused non-apoptotic cell death.

Before we performed these experiments, we choose buprenorphine hydrochloride (Bph), a clinically used analgesic, as the positive control for an apoptosis-inducing drug in MCF-7 cells (Kugawa et al. 2004a, b). Interestingly, neither DXR nor C + D + F induced DNA ladder formation in the low-molecular-weight range nor did they cause nuclear heterochromatin condensation. Furthermore, the flow-cytometric analysis of MCF-7 cells treated with DXR or C + D + F generated similar FACS cytograms that were completely different from the cytograms for MCF-7 cells treated with CPA, 5-FU, or Bph (the positive control; Kugawa et al. 2004b). These differences in the dying cells' characteristics led us to investigate the nature of the MCF-7 cell death induced by DXR and C + D + F.

Mitochondria are key organelles in classic apoptosis (Green et al. 2011; Martinou and Youle 2011; Wlodkowic et al. 2011; Lemarie and Grimm 2011). Specifically, destruction of the mitochondrial membrane potential is a trigger event for the mitochondrial apoptosis pathway. The release of mitochondria-originated cytochrome *c* and/or SMAD/DIALBO activates downstream caspases, such as caspase, 6, 7, and 9, which in turn activate capase-3. We speculated that a close investigation of mitochondrial structure might reveal clues to the different type of cell death observed in DXR- and C + D + F-treated MCF-7 cells, regardless of whether the induced cell death was apoptotic.

As a first step toward answering this question, we examined the entire cell structure, especially focusing on the mitochondrial morphology, in MCF-7/pDsRed2-Mito cells after administration of the three anticancer drugs and of Bph (as the positive

control). Unlike with CPA and 5-FU administration, the characteristic morphology of red-glowing mitochondria was observed with DXR and C + D + F administration, as expected. Therefore, we further investigated the detailed morphology of dying MCF-7/pDsRed2-Mito cells using electron microscopy. The electron microscopy images strongly suggested that the nuclear membrane might be involved in the DXR- and C + D + F-induced form of cell death.

2. Investigations, results and discussion

2.1. Morphology of the mitochondrial structure and nuclear membrane in intact MCF-7/pDsRed2-Mito cells

In our previous study (Kugawa et al. 2004a), to investigate the role of mitochondria in Bph-induced cell death of the human breast cancer cell line MCF-7, we constructed MCF-7/pDsRed2-Mito cells by introducing the pDsRed2-Mito® vector into MCF-7 cells. The pDsRed2-Mito® expression vector includes the DsRed2® red-fluorescing protein sequence and a mitochondrial targeting sequence from subunit VIII of human cytochrome *c* oxidase (see Clontech's home page; http://www.clontech.com.) that causes the mitochondria in the MCF-7/pDsRed2-Mito cells to fluoresce red, under stimulation with an IX-FLA® fluorescence device.

Fig. 1 shows the fluorescence images of intact MCF-7/pDsRed2-Mito cells. The dot-like mitochondria were uniformly distributed in the cytoplasm (Fig. 1-A). The electron microscopic image showed a normal nucleus structure and cell organellae, including the lysosome and mitochondria (Fig. 1-B). Even at high magnification, × 20,000 (Fig. 1-C) and × 50,000 (Fig. 1-D), the cell membrane and mitochondrial membrane were clearly intact.

2.2. Morphology of the mitochondrial structure and nuclear membrane in Bph-treated MCF-7/pDsRed-Mito cells

Fig. 2 shows both fluorescence and electron microscopic images of Bph-treated MCF-7/pDsRed2-Mito cells, one day (D1) after Bph treatment (Bph D1). The analgesic Bph was adopted as a positive control for the physical destruction of mitochondria, which is associated with apoptosis-like cell death in MCF-7 cells (Kugawa et al. 2004a). After the administration of 100 μM Bph, round cells that uniformly fluoresced red were observed (Fig. 2-A). The DsRed2-Mito® protein has an N-terminal mitochondrial targeting sequence from cytochrome *c* oxidase subunit VIII. Thus, the uniform red fluorescence in the MCF-7/DsRed2-Mito cells resulted when the complete destruction of the mitochondrial membrane released the cytochrome *c*-conjugated DsRed2-Mito® into the cytoplasm.

Interestingly, unlike in the intact MCF-7/pDsRed2-Mito cell image (Fig. 1-A), all of the cells we observed on Bph D1 were "uniformly glowing round" (or UGR) cells, and the dark shape caused by the nucleus near the center of the intact cells was not observed at all (Fig. 2-A). One explanation for this observation is that, by Bph D1, the nuclear membrane had been destroyed, although the cell membrane remained intact. Alternatively, the nucleus might have shrunk, and therefore become hidden by the red-glowing cytoplasm. Or, third, the nuclear membrane may have become leaky enough to allow the DeRed2-Mito® protein to diffuse inside the nucleus. In our previous report (Kugawa et al. 2004b), we observed Hoechst 33258 (which binds to DNA and fluoresces blue)-stained MCF-7 cells, and found that nuclear heterochromatin blebbing, a characteristic feature of apoptosis (Galluzzi et al. 2007), had occurred by Bph D1. This is strong supporting evidence for the final possibility above. Therefore, we conducted an electron microscopic observation and carefully examined the nuclear structure (Fig. 2-B, 2-C, 2-D).

Bph D1 is a critical time for observing the apoptosis of MCF-7 cells, because the apoptosis-like cell death caused by Bph progresses so rapidly that almost no living cells can be seen at Bph D2. In contrast, cell death progressed slowly when the cells were treated with CPA, DXR, 5-FU, or C + D + F cells (Kugawa et al. 2004b). Therefore, Bph D1 was chosen as the appropriate sampling point for investigating the morphology of dying cells, when using Bph as the positive control.

In the electron microscopy images of Bph D1 cells, the cell membrane had maintained its structure (see arrow #1 in Fig. 2-B, 2-C). In contrast, the nuclear membrane was about to deteriorate (× 4,000, Fig. 2-B; × 7,000, cells at right in Fig. 2-C) or visible deterioration had already begun (× 7,000, cell at left in Fig. 2-C). In addition, only traces of mitochondrion fragments were detectable in some samples (arrow #4 in Fig. 2-B and 2-D), the nuclear structure was marked by condensed chromatin (arrow #3 in Fig. 2-B, 2-C, and 2-D), an apoptosis characteristic. Conclusively, in the Bph-induced UGR cells, the damage to the mitochondria was so great that the mitochondrial contents were strewn throughout the cytoplasm. In addition, the leaky nuclear membrane apparently could no longer function as a barrier between the cytoplasm and the nucleus, causing the UGR fluorescent phenotype (Fig. 2-A).

2.3. Effect of individual or combined treatment of MCF-7/pDsRed2-Mito cells with anti-cancer drugs on the distribution of red fluorescence

The cell death rate in the two days after the administration of any of the three anticancer drugs was about 90% to 50% (Kugawa et al. 2004b). Fig. 3 shows the morphology of the red-glowing dying cells after the administration of anticancer drugs. By conducting close observation of the cells, we recognized three patterns of fluorescence distribution (Fig. 3): the UGR cells, described above (Fig. 2), the "two separated glow" (or TSG) cells, and the "irregular glowing" (or IG) shape. IG cells were dominant in CPA D2 (Fig. 3-A) and 5-FU D2 (Fig. 3-C) samples. We were particularly interested in the TSG cells' novel shape, which was dominant in the DXR D2 samples (Fig. 3-B). A simple explanation of this characteristic feature is that COX VIII enzyme from the mitochondria was actively distributed to two opposite sites in the cell, or that some unknown structure in the center of the cells interfered with DsRed2-Mito®'s uniform distribution. Almost 90% of the cells in the DXR D2 sample were TSG. The TSG cells were also dominant in the C + D + F sample at D2 (Fig. 3-D), with few IG cells. This was interesting, because the cytotoxic effect of CPA and 5-FU can be masked by DXR, which has an overwhelming cytotoxic effect in multiple-drug administration (C + D + F). The effects of DXR were also dominant over the effects of CPA and 5-FU in DNA ladder formation, the DNA fragmentation assay, and FACS analysis in our previous study (Kugawa et al. 2004b). For example, the FACS cytogram of the C + D + F samples closely resembles that of DXR (Kugawa et al. 2004b).

Thus, we next conducted electron microscopy experiments to investigate the morphology of cells dying from the actions of these anticancer drugs.

2.4. Electron microscopy of the IG cells observed in the CPA D2 sample

The results of electron microscopy of the CPA D2 sample are shown in Fig. 4. Some typical features were observed; i.e., the cell membrane seemed to be intact (arrow #1, Fig. 4-A) or

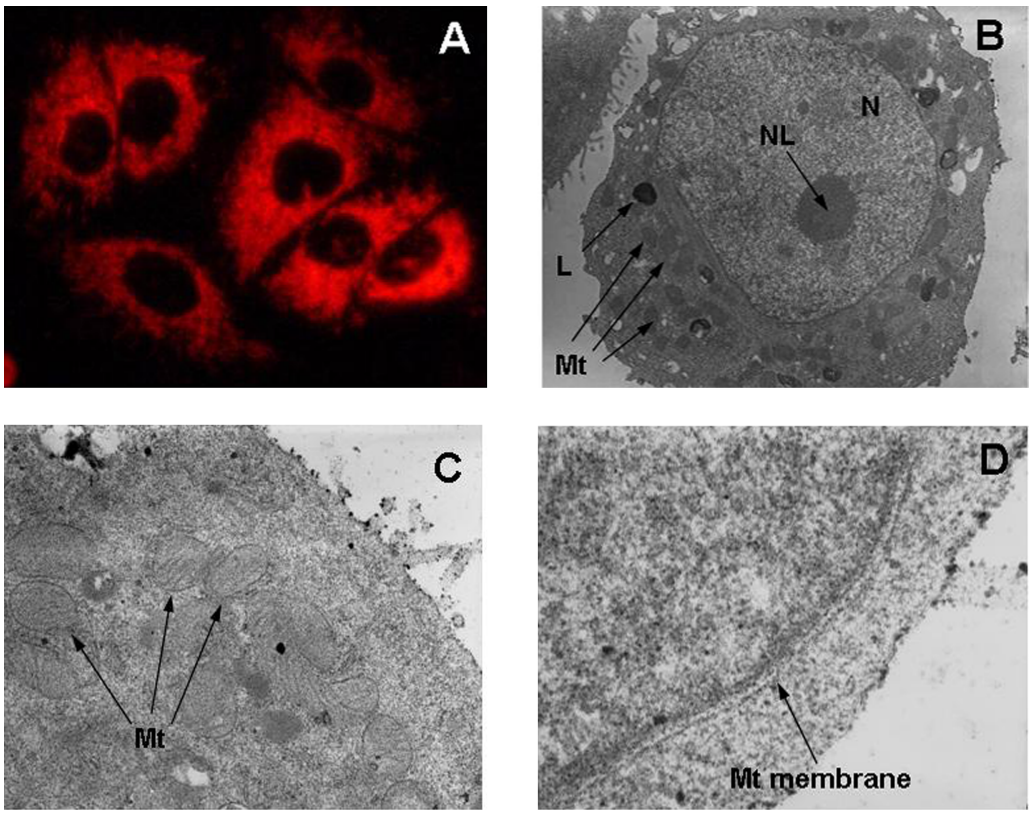

Fig. 1: Morphology of intact MCF-7/pDsRed2-Mito cells, A, Fluorescence image of intact MCF-7/pDsRed2-Mito cells (× 400 magnification). B, Electron microscopic image of an intact whole cell (× 6,000). C, Electron microscopic image of mitochondria (× 20,000). D, Electron microscopic image showing part of a mitochondrial membrane (× 50,000). N, nucleus; NL, nucleolus; L, lysosome; and Mt, mitochondria

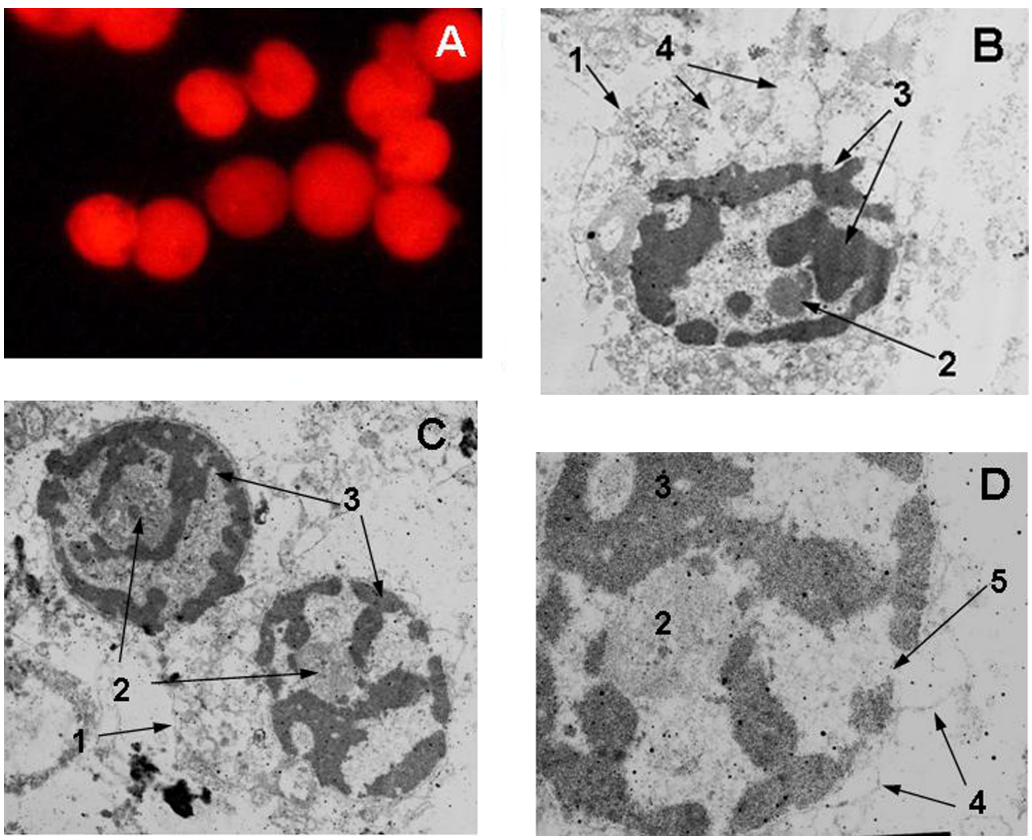

Fig. 2: Morphology of Bph-treated MCF-7/pDsRed2-Mito cells, A, Fluorescence image of Bph-treated MCF-7/pDsRed2-Mito cells (× 400). B, Electron microscopic image of a whole Bph-treated cell (× 4,000). C, Electron microscopic images of nuclei from Bph-treated cells (× 7,000). D, Detailed view of the nucleus (× 20,000). Arrows: #1, cell membrane; #2, nucleus; #3, condensed heterochromatin; #4, residue of destroyed Mt; and #5, an opening in the nucleus

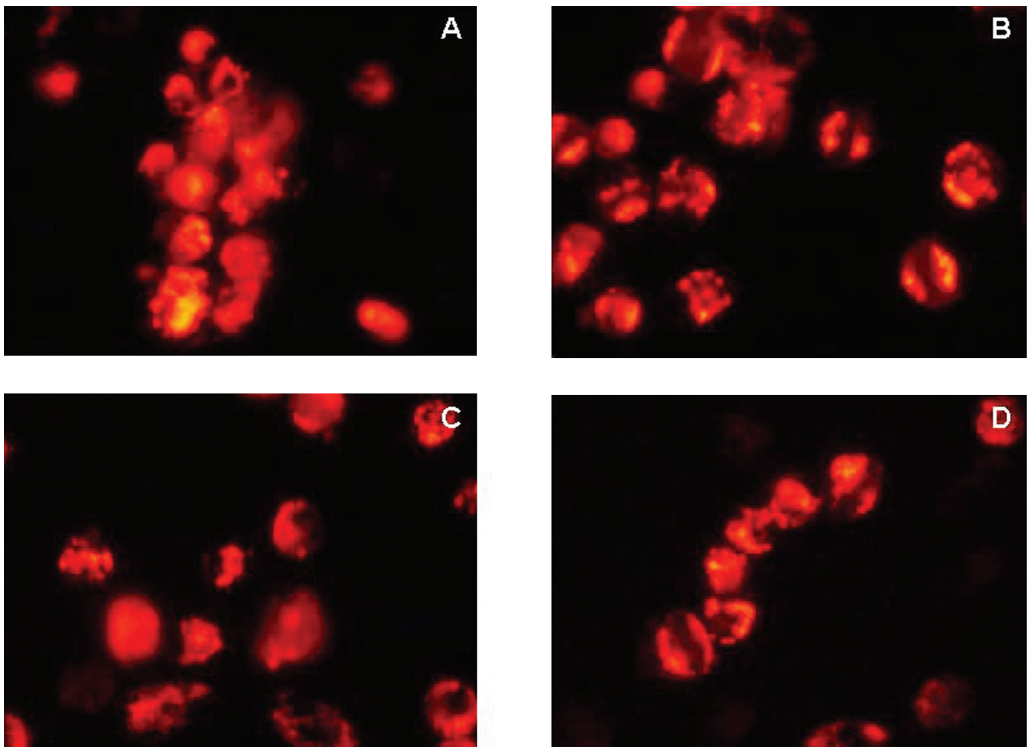

Fig. 3: MCF-7/pDsRed2-Mito cells after individual or combined treatment with the three anticancer drugs, Fluorescence images of MCF-7/pDsRed2-Mito cells treated with CPA (A), DXR (B), 5-FU (C), or C + D + F (D). Magnitude is ×400

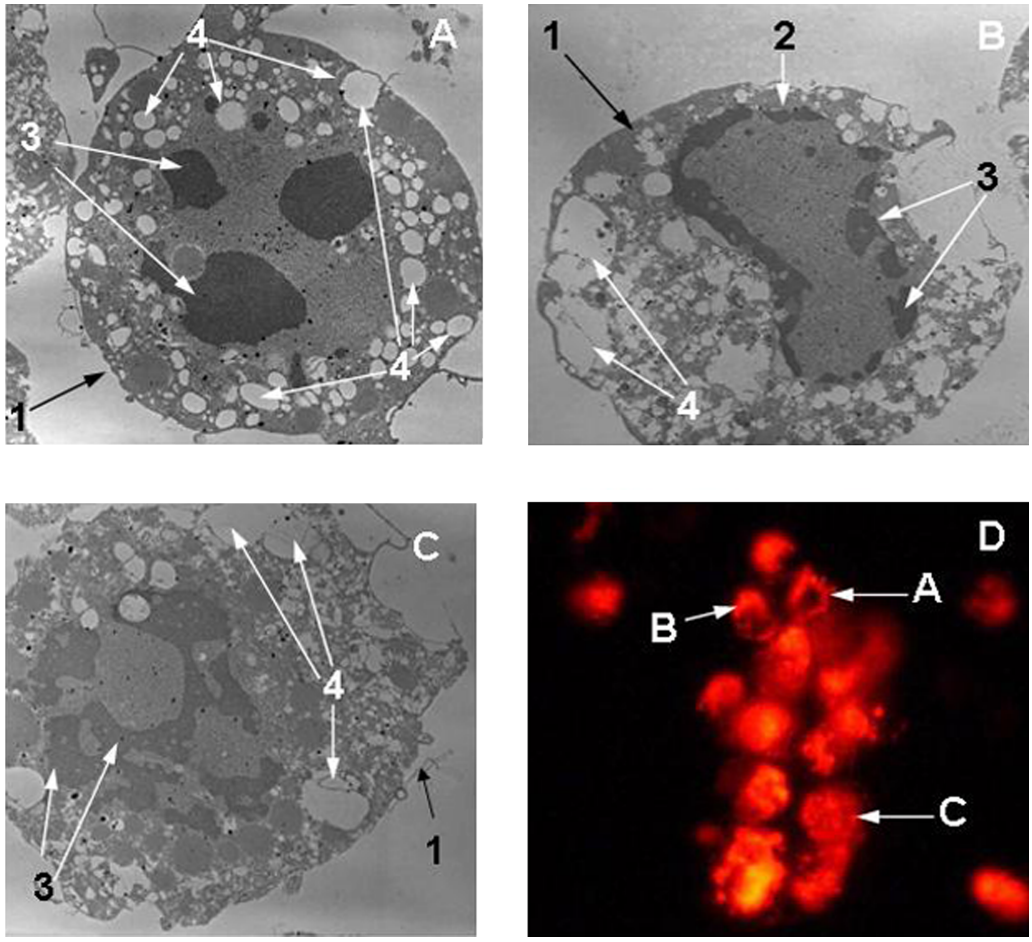

Fig. 4: IG cells among the CPA-treated MCF-7/pDsRed2-Mito cells, A, B, and C, electron microscopic images of CPA-treated MCF-7/pDsRed2-Mito cells. A; × 5,000, B; × 4,000, C; × 5,000. D is the same image as in Fig. 3-A, and shows fluorescent CPA D2 cells. Arrows #1, #2, #3, and #4 indicate cell membrane, nuclear membrane, condensed heterochromatin, and large vacuoles, respectively. The arrows A, B, and C in panel D point out cells with the representative morphology of those shown in the electron microscopy images in panels A, B, and C

slightly damaged (arrow #1, Fig. 4-B, 4-C). Condensed heterochromatin, which is a typical feature of apoptosis, was clearly observed (arrow #3, Fig. 4-A, 4-B, and 4-C). However, the nuclear membrane was partially damaged (arrow #2, in Fig. 4-B, 4-C) or had almost disappeared (Fig. 4-A). A likely explanation for the variability in nuclear shapes is that the cells were in the early phase of apoptosis at D2.

Another distinguishing feature of this CPA D2 sample is the presence of many blebs and relatively large vacuoles in the cell cytoplasm (arrow #4, Fig. 4-A, 4-B, and 4-C). This finding is consistent with an earlier investigation by Yoon et al. using epithelial cells from the rat thymus cortex (Yoon et al. 1997). Similar structures were also slightly seen in the Bph D1 cells (data not shown). These structures could represent a mixture of first-stage cytolysis and kariolysis. Some structural damage to mitochondria was observed, but its extent was less than that in the Bph D1 samples (data not shown). Note the arrows A, B, and C in panel D point out cells with the representative morphology of those shown in the electron microscopy images in panels A, B, and C.

2.5. Electron microscopy of the IG cells observed in 5-FU D2 cells

In general, the 5-FU D2 cells seemed to have relatively rigid cell membranes (arrow #1 in Fig. 5-A, 5-B), and the dying cells retained their round shape (Fig. 5-D). The nuclear structures showed variable morphology. Some had an irregular shape with a deteriorating nuclear membrane (arrow #2 in Fig. 5-A). Others appeared to have an almost intact nuclear membrane (arrow #2 in Fig. 5-B). The arrows labeled A and B in panel Fig. 5-D show representative cells with an irregularly shaped nucleus those shown in the electron microscopy images in panels A and B. Heterochromatin blebbing was also detected in these cells, but it was less expansive than in other specimens such as Bph D1 or CPA D2.

The mitochondrial structure showed an interesting feature. As shown in Fig. 5-A (× 3,000) and Fig. 5-B (× 7,000), the mitochondria had obviously swelled and the cristae and lamellar structure were hard to detect, even at × 15,000 magnification (Fig. 5-C). This is the typical appearance of "swollen mitochondria" that have almost completely lost the mitochondrial membrane potential (Shinohara et al. 1998, 2002; Klein et al. 2011). Therefore, a large portion of the mitochondrial internal components had leaked into the cytosol, but the mitochondrial membrane had managed to keep its structure. For this reason, the 5-FU D2 cells exhibited an uneven fluorescence intensity in their cytoplasm (Fig. 5-D), unlike the Bph D1 cells (Fig. 2-A).

2.6. Electron microscopy of the TSG cells observed in the DXR D2 sample

The TSG ("two-separated glowing") phenotype is obvious in Fig. 6-D. With few exceptions, all the cells in the DXR D2 sample showed this feature. Fig. 6-A and 6-B shows relatively low-magnification (A, × 4,000; B, × 6,000) electron microscopic images of these cells. Both the cell and nuclear membrane were clearly visible and intact, and the nucleus did not take up a large volume in the cell. The nuclei also tended to be a bit off-center, i.e., positioned more on one side of the cell (Fig. 6-A and 6-B). Some interesting features of the mitochondria were visible. First, most of the mitochondria were gathered on one side of each cell (arrow #4 in Fig. 6-A and 6-B). Second, the mitochondrial structure had changed from the intact rod-like shape to become round (Fig. 6-C). Third, the cristae and lamellar structure had disappeared; instead, small vesicles were present inside the mitochondria (arrow #5 in Fig. 6-C). Thus, some kind of damage to the mitochondria had been caused by DXR. However, at least by morphological observation, the damage was different from that caused by Bph (compare the mitochondrial images in Fig. 2 and 6). Peng et al. subtyped the mitochondrial structures seen in CHO cells treated with different types of apoptosis-inducing drugs (Peng et al. 2011). According to those authors, there are six mitochondrial morphologies, and the typical mitochondria in Fig. 6-C could be classified as the "swollen globules" type, a morphology that immediately precedes "mitochondrial degradation."

Taking all the above morphological observations into consideration, we conclude that 1) in the DXR D2 samples, the mitochondrial membrane was barely preserved, but its permeability was substantially increased, allowing enzymes such as COX VIII to leak into the cell cytoplasm. 2) The nucleus itself became relatively bigger than in intact cells, but its membrane seemed to retain its function, thus preventing the DsRed2-Mito® protein from diffusing into the nucleus. The TSG phenotype, therefore, is attributable to the intact nuclear membrane, which causes the nucleus to appear as a dark structure that divides the glowing cytoplasm.

2.7. Electron microscopy of the TSG cells in the C + D + F D2 sample

For the C + D + F D2 sample, CPA, DXR, and 5-FU were simultaneously administered to the MCF-7/pDsRed2-Mito cells. A possible outcome of the combined drug treatment was that the cells' morphology would reflect a mixture of the effects of the individual drugs. For example, one third of the cells might show features of the CPA D2 sample, another third might show features of the 5-FU D2 sample, and the rest would resemble the DXR D2 sample. However, almost more than 90% of the cells were TSG cells. A representative microscopic field is shown in Fig. 7-D . The arrows A and B indicate representative cells, with the same morphologies as those shown in Fig. 7-A and 7-B. We also reported the above-described phenomenon in other experiments (Kugawa et al. 2004b). The most plausible explanation for this phenomenon is that it reflects the difference in cytotoxicity among the three anticancer drugs: DXR is the most cytotoxic, 5-FU is second, and CPA is third (Kugawa et al. 2004b).

The electron microscopic observation of the TSG cells revealed a very different story (see Fig. 7-A, 7-B, and 7-C). Fig. 7-A and 7-B shows TSG cells at × 4,000 and × 7,000 magnification, respectively, in which very distinguishable vesicles or blebs were easily detected (arrow #5). Such vesicles or blebs were plentiful in the CPA D2 cells (Fig. 4), which appeared as IG cells by fluorescence microscopy. Furthermore, the TSG cells that were representative of DXR D2 cells did not show these structures in the cytoplasm (see Fig. 6-A, 6-B); instead, they had bleb-like structures in the mitochondria (see, Fig. 6-C).

The cell membrane of the C + D + F D2 cells appeared to be intact (Fig. 7-A and 7-B), and the nuclear membrane somehow managed to keep its structure (Fig. 7-A) or was near to breaking (Fig. 7-B). The heterochromatin condensation was clearly observed in Fig. 7-B. In contrast, the damage to the mitochondria was critical. In the relatively low-magnification images (× 4,000 in Fig. 7-A, × 9,000 in Fig. 7-B), the mitochondria were very hard to distinguish from the blebs. In the high-magnification image (× 30,000 in Fig. 7-C), the mitochondria were finally detectable, but their structure was completely different from that of intact mitochondria (arrow #4 in Fig. 7-C), in that they had swollen into a round shape, and the interior structure had completely disappeared. In addition, the mitochondrial membrane seemed to become thin. This characteristic mitochondrial mor-

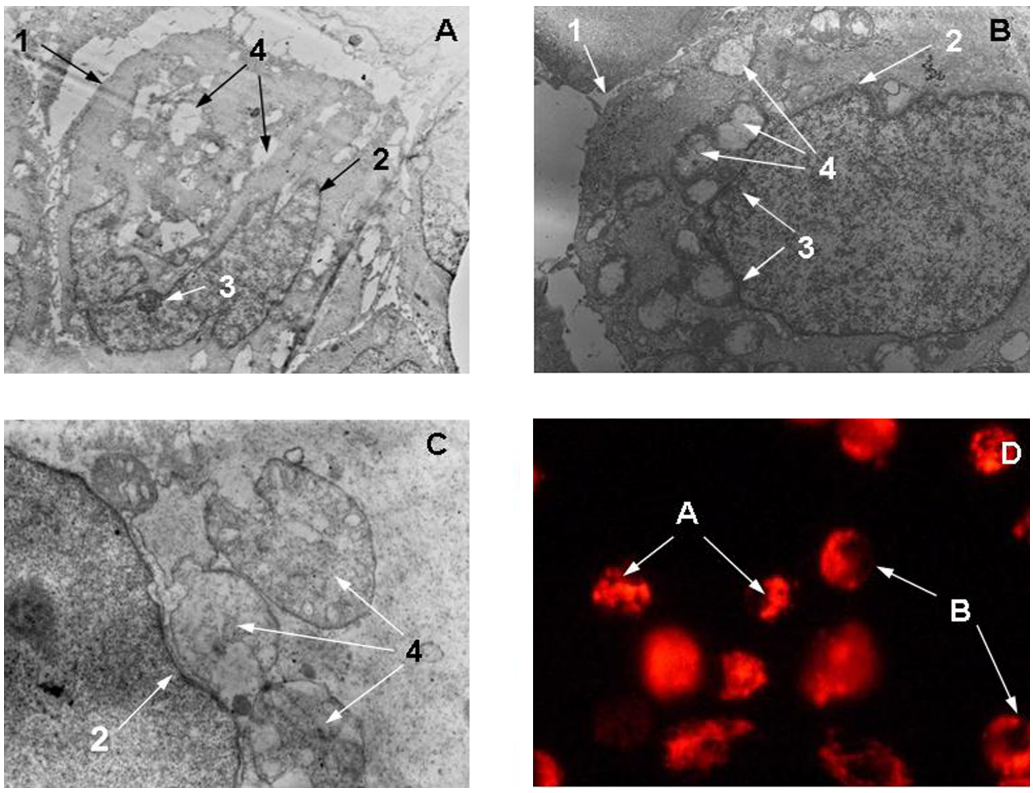

Fig. 5: IG cells observed in the 5-FU-treated MCF-7/pDsRed2-Mito cells, A, B, and C, show electron microscopic images of 5-FU-administered MCF-7/pDsRed2-Mito cells. A; × 3,000, B; × 7,000, C; × 15,000 respectively. D is the same image as in Fig. 3-C, and shows fluorescent 5-FU D2 cells. Arrows #1, #2, #3, and #4 indicate cell membrane, nuclear membrane, condensed heterochromatin, and mitochondria, respectively. Arrows A and B in panel D indicate representative cells of the morphology shown in the electron microscopy images in panels A and B

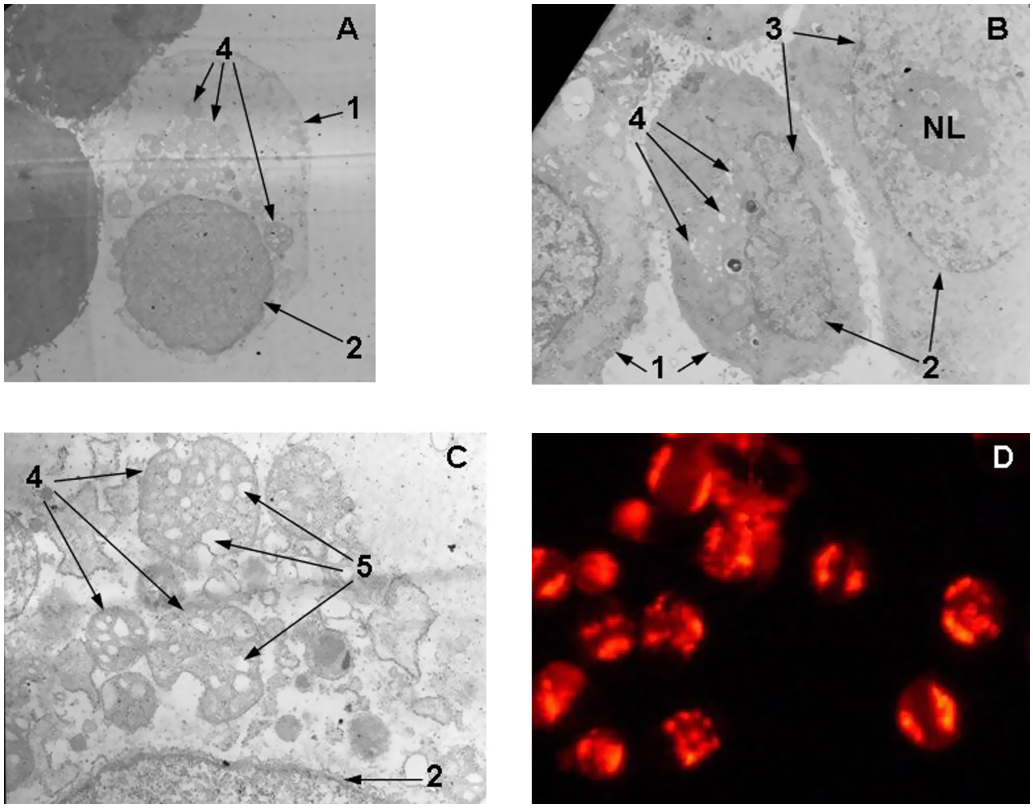

Fig. 6: TSG cells observed in the DXR-treated MCF-7/pDsRed2-Mito cells, A, B, and C, show electron microscopic images of DXR-treated MCF-7/pDsRed2-Mito cells. A; × 6,000, B; × 6,000, C; × 15,000 respectively. D is the same picture as shown in Fig. 3-B, showing fluorescent DXR D2 cells. Arrows #1, #2, #3, #4, and #5 indicate cell membrane, nuclear membrane, condensed heterochromatin, mitochondria, and small vesicles in the mitochondria, respectively. A and C show the same specimen

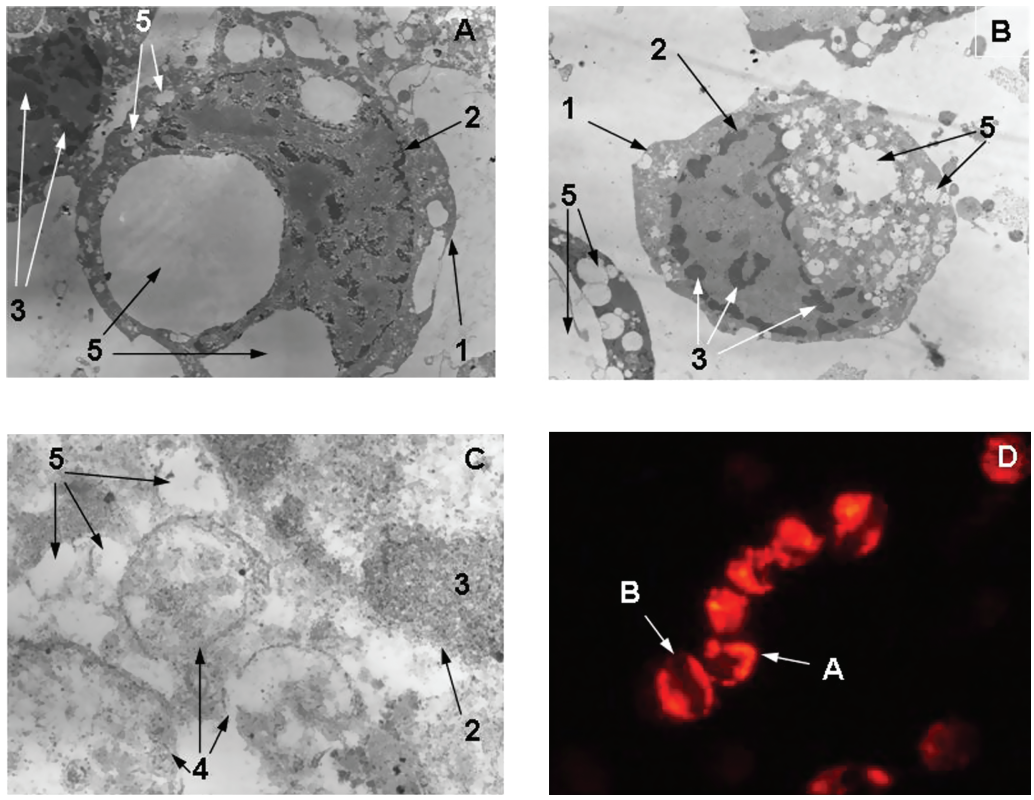

Fig. 7: TSG cells observed in C + D + F-treated MCF-7/pDsRed2-Mito cells, A, B, and C show electron microscopic images of cells treated with all three anti-cancer drugs (C + D + F). A; × 4,000, B; × 9,000, C; × 30,000 respectively. D is the same image as shown in Fig. 3-D, and shows fluorescent C + D + F D2 cells. Arrows #1, #2, #3, #4, and #5 indicate cell membrane, nuclear membrane, condensed heterochromatin, mitochondria, and small vesicles in the cytoplasm, respectively. Arrows A and B in panel D indicate representative cells of the kind shown in the electron microscopy images in panels A and B

phology would probably be classified as the "swollen globule" type in Peng's subtyping (Peng et al. 2011).

These observations suggest that the TSG cells in the C + D + F D2 sample were completely different from the TSG cells observed in the DXR D2 sample. That is, even though the morphology appeared identical by fluorescence microscopy, the events occurring inside the MCF-7/pDsRed2-Mito cells were different.

The present study focused on the morphology of dying human breast cancer cells treated with clinically used anticancer drugs. The dying cells expressed some typical apoptotic features under electron microscopic observation. In 2007, the morphological characterization of cell death was defined by the Nomenclature Committee on Cell Death in *Cell Death and Differentiation* (Galluzzi et al. 2007). According to their criteria, the CPA D2 and C + D + F D2 cell death might be classified as autophagic cell death (type 2). The use of a cell line with constitutively red-glowing mitochondria allowed us to observe the morphological details of dying human breast cancer cells. This morphological study may serve as the basis for molecular biology-based investigations of the dying mechanisms of cancer cells, which may contribute to the development of future cancer chemotherapies.

3. Experimental

3.1. Cell culture and fluorescence observation

The MCF-7/pDsRed2-Mito cells are a subclone of the MCF-7 human breast cancer cell line, and were described previously (Kugawa et al. 2004a). The cells were cultured in Dulbecco's Modified Eagle's Medium (Nissui; Tokyo, Japan) supplemented with 10% fetal bovine serum, 100 U/ml penicillin (Meiji; Tokyo, Japan) and 100 μg/ml streptomycin (Meiji; Tokyo, Japan). The cells were grown under 100% humidity in a 5% CO_2 incubator at 37 °C. The morphological observation was conducted using an Olympus model IX-70 inverted phase-contrast microscope (Olympus; Tokyo, Japan) equipped with an IX-FLA fluorescence observation device.

3.2. Cell death induction

The three anticancer drugs CPA, DXR, and 5-FU were added alone or in combination to logarithmically growing MCF-7/pDsRed-2 Mito cells at a final concentration of 500 μg/ml CPA, 5 μg/ml DXR, and 25 μg/ml 5-FU. Bph, the positive control, was added to a final concentration of 100 μM (from a 40% methanol stock solution). These concentrations were determined with reference to the clinical dosage as explained previously (Kugawa et al. 2004b). Cell images were taken 1 day after drug administration (D1) or D2, as described in the text. All chemicals used were superfine grade and purchased from Sigma (MO, USA).

3.3. Transmission electron microscopy

MCF-7/pDsRed2-Mito cells were incubated in fixative (4% glutaraldehyde in 0.1 M cacodylate, pH 7.2) for 45 min at room temperature. The cells were scraped off the plates and transferred to microcentrifuge tubes, spun down, and washed with 0.1 M cacodylate buffer. Cells were prefixed in 1.0% OsO_4 with 0.1% potassium ferrocyanide until the pellet turned brown, washed with 0.15 M NaCl three times for 5 min each, and then stained en-block with 0.5% Mg uranyl acetate in 0.15 M NaCl for 1 h at room temperature. Cells were washed with 0.15 M NaCl followed by a series of 10-min graded ethanol washes. The pellet was mixed with 100% ethanol with Epon (2:1) and incubated on a rotator for 24 h, changed to 100% ethanol with Epon (1:1) for 8 h, and then moved to pure Epon 16 h. Pellets were embedded in Epon capsules for 48 h at 65 °C. Ultrathin sections were cut on a LKB BROMMA Ultratome-V 2088 and stained with uranyl acetate and lead citrate. Specimens were examined using a Hitachi H-800 transmission electron microscope with real-time digital imaging.

References

Derenzini M, Brighenti E, Donati G, Vici M, Cecccarelli C, Santini D, Taffurelli M, Montanaro L, Treré D (2009) The p53-mediated sensitivity of cancer cells to chemotherapeutic agents is conditioned by the status of the retinoblastoma protein. J Pathol 219: 373–382.

Galluzzi L, Maiuri MC, Vitale I, Zischka H, Castedo M, Zitvogel L, Kroemer G (2007) Cell death modalities: classification and pathophysiological implications. Cell Death Differ 14: 1237–1243.

Green DR, Galluzzi L, Kroemer G (2011) Mitochondria and the autophagy-infalmmation-cell death axis in organismal aging. Science 333: 1109–1112.

Klein B, Wörndl K, Lütz-Meindl U, Kerschbaum HH (2011) Perturbation of intracellular K^+ homeostasis with valinomycin promotes cell death by mitochondria swelling and autophagic processes. Apoptosis 16: 1101–1117.

Kugawa F, Matsumoto K, Aoki M, (2004a) Apoptosis-like cell death of human breast cancer cell line MCF-7 induced by buprenorphine hydrochloride. Life Sciences 75: 287–299.

Kugawa F, Ueno A, Kawasaki M, Aoki M (2004b) Evaluation of cell death caused by CDF (cyclophosphamide, doxorubicin, 5-fluorouracil) multidrug administration in the human breast cancer cell line MCF-7. Biol Pharm Bull 27: 392–398.

Lemarie A, Grimm S (2011) Mitochondrail respiratory chain complexes: apoptosis sensors mutated in cancer? Oncogene 30: 3985–4003.

Martinou JC, Youle RJ (2011) Mitochondria in apoptosis: Bcl-2 family members and mitochondrial dynamics. Dev Cell 21: 92–101.

Nagar S (2010) Parmacokinetics of anti-cancer drugs used in breast cancer chemotherapy. Adv Exp Med Biol 678: 124–132.

Pal SK, Mortimer J (2009) Adjuvant chemotherapy for older adults with breast cancer: making the standard a standard. Womens Health (Lond Engl) 5: 481–484.

Peng JY, Lin CC, Chen YJ, Kao LS, Liu YC, Chou CC, Huang YH, Chang FR, Wu YC, Tsai YS, Hsu CN (2011) Automatic morphological subtyping reveals new roles of caspases in mitochondrial dynamics. PLoS Comput Biol 7: e1002212.

Perez E, Muss HB (2005) Optimizing adjuvant chemotherapy in early-stage breast cancer. Oncology (Williston Park) 19: 1759–1767.

Perik PJ, De Vries EG, Boomsma F, Messerschmidt J, Van Veldhuisen DJ, Sleijfer DT, Gietema JA, Van der Graaf WT (2006) The relation between soluble apoptotic proteins and subclinical cardiotoxicity in adjuvant-treated breast cancer patients. Anticancer Res 26: 3803–3811.

Shinohara Y, Bandou S, Kora S, Kitamura S, Inazumi S, Terada H (1998) Cationic uncouplers of oxidative phosphorylation are inducers of mitochondrial permeability transition. FEBS Lett 428: 89–92.

Shinohara Y, Almotif MR, Yamamoto T, Ishida T, Kita F, Kanzaki H, Ohnishi M, Yamashita K, Shimizu S, Terada H (2002) Permeability transition-independent release of mitochondrial cytochrome *c* induced by valinomyacin. Eur J Biochem 269: 5224–5230.

Tokudome N, Ito Y (2006) Adjuvant chemotherapy based on evidence-based medicine for breast cancer patients. Gan To Kagaku Ryoho 33: 318–323.

Végran F, Boidot R, Oudin C, Riedinger JM, Bonnetain F, Lizard-Nacol S (2006) Overexpression of caspase-3 s splice variant in locally advanced breast carcinoma is associated with poor response to neoadjuvant chemotherapy. Clin Cancer Res 12: 5794–5800.

Wlodkowic D, Telford W, Skommer J, Darzynkiewicz Z (2011) Apoptosis and beyond: cytometry in studies of programmed cell death. Methods Cell Biol 103: 55–98.

Yoon S, Yoon YH, Kim BS, Kim JJ (1997) Ultrastructural alternations of the cortical epithelial cells of the rat thymus after cyclophoshamide treatment. Histol Histopathol 12: 401–413.

Zhang F, Aft RL (2009) Chemosensitizing and cytotoxic effects of 2-deoxy-D-glucose on breast cancer cells. J Cancer Res Ther 5 Suppl 1: S41–43.